

1 **Benchmark seasonal prediction skill estimates based on regional indices**

2 John E. Walsh¹, J. Scott Stewart², Florence Fetterer²

3 ¹Alaska Center for Climate Assessment and Policy, University of Alaska, Fairbanks, AK 99709 USA

4 ²National Snow and Ice Data Center, University of Colorado, Boulder, CO 80303 USA

5 *Correspondence to:* John E. Walsh (jewalsh@alaska.edu)

6 **Abstract.** Basic statistical metrics such as autocorrelations and across-region lag correlations of
7 sea ice variations provide benchmarks for the assessments of forecast skill achieved by other
8 methods such as more sophisticated statistical formulations, numerical models, and heuristic
9 approaches. In this study we use observational data to evaluate the contribution of the trend to the
10 skill of persistence-based statistical forecasts of monthly and seasonal ice extent on the pan-Arctic
11 and regional scales. We focus on the Beaufort Sea where the Barnett Severity Index provides a
12 metric of historical variations in ice conditions over the summer shipping season. The variance
13 about the trend line differs little among various methods of detrending (piecewise linear, quadratic,
14 cubic, exponential). Application of the piecewise linear trend calculation indicates an acceleration
15 of the winter and summer trends during the 1990s. Persistence-based statistical forecasts of the
16 Barnett Severity Index as well as September pan-Arctic ice extent show significant statistical skill
17 out to several seasons when the data include the trend. However, this apparent skill largely
18 vanishes when the data are detrended. In only a few regions does September ice extent correlate
19 significantly with antecedent ice anomalies in the same region more than two months earlier. The
20 springtime “predictability barrier” in regional forecasts based on persistence of ice extent
21 anomalies is not reduced by the inclusion of several decades of pre-satellite data. No region shows
22 significant correlation with the detrended September pan-Arctic ice extent at lead times greater
23 than a month or two; the concurrent correlations are strongest with the East Siberian Sea. The
24 Beaufort Sea’s ice extent as far back as July explains about 20% of the variance of the Barnett
25 Severity Index, which is primarily a September metric. The Chukchi Sea is the only other region
26 showing a significant association with the Barnett Severity Index, although only at a lead time of
27 a month or two.

28 **1 Introduction**

29 One of the most widely monitored variables in the climate system is Arctic sea ice. By any
30 measure, Arctic sea ice has decreased over the past few decades (Box et al., 2019). September
31 sea ice extent during the past 5-10 years has been approximately 50% of the mean for the 1979-
32 2000 period (AMAP, 2017). The recent decline is unprecedented in the satellite record, in the
33 period of direct observations dating back to 1850 (Walsh et al., 2016), and in paleo
34 reconstructions spanning more than 1400 years (Kinnard *et al.*, 2011). The recent reduction of
35 sea ice has been less in winter and spring than in summer and autumn, resulting in a sea ice cover
36 that is largely seasonal (AMAP, 2017). The increasingly seasonal ice cover contrasts with the
37 Arctic Ocean's predominantly multiyear ice pack of the pre-2000 decades. When compared to
38 the reductions of the spatial extent of sea ice, the percentage reductions of ice volume and
39 thickness are even larger. Ice thickness decreased by more than 50% from 1958-1976 to 2003-
40 2008 (Kwok and Rothrock, 2009), and the percentage of the March ice cover made up of thicker
41 multiyear ice (ice that has survived a summer melt season) decreased from 75% in the mid-1980s
42 to 45% in 2011 (Maslanik *et al.*, 2011). Laxon et al. (2013) indicate a decrease of 64% in autumn
43 sea ice volume from 2003-08 to 2012. The portion of the Arctic sea ice cover comprised of older
44 thicker ice has decreased from 45% in 1985 to 21% in 2017 (NOAA, 2018).

45 While the loss of sea ice is generally presented in terms of pan-Arctic metrics, regional
46 trends can be quite different from the pan-Arctic trends. The Bering Sea, for example, showed a
47 positive trend of coverage (fewer open water days) from 1979 through 2012 (Parkinson, 2014),
48 However, the positive trend of Bering Sea ice largely vanishes when the most recent winters
49 (especially 2017-18) are included. By contrast, the Chukchi and Beaufort Seas to the north of
50 the Bering Sea have shown some of the largest decreases of summer ice coverage in the entire
51 Arctic (Onarheim et al., 2018). Another area of strong decrease of ice coverage has been the
52 Barents/Kara Sea region.

53 The Beaufort Sea serves as an illustrative example of the impacts of trends and variability
54 of sea ice. The number of open water days immediately offshore of the Beaufort coast has been
55 60-120 in recent years. Parkinson's (2014) Figure 2 shows that the number of open water days
56 increased by 20-30 days per decade over the period 1979-2013. However, as recently as the
57 1970s, there were summers with little or no open water in this region, as described by Crowley
58 Maritime, one of the major barge operators in the Alaska region:

59 “With pipeline construction well underway in 1975, the Crowley summer sealift
60 flotilla to the North Slope faced the worst Arctic ice conditions of the century. In fleet
61 size, it was the largest sealift in the project's history with 47 vessels amassed to carry
62 154,420 tons of cargo, including 179 modules reaching as tall as nine stories and
63 weighing up to 1,300 tons each. Vessels stood by for nearly two months waiting for the
64 ice to retreat. Finally in late September the ice floe moved back and Crowley's tugs and
65 barges lined up for the slow and arduous haul to Prudhoe Bay. When the ice closed again,
66 it took as many as four tugs to push the barges, one at a time, through the ice”.

67 — *From Crowley Maritime, 50 Years of Service in Alaska (2002)*

68 As will be shown, the contrast between present-day ice conditions and the Crowley
69 experience of the 1970s is largely a manifestation of the trend of Beaufort Sea ice cover.
70 However, sea ice also exhibits large year-to-year variability, which has been superimposed on
71 the recent trend towards less sea ice in the Arctic. This variability challenges users of coastal
72 waters in various sectors and lies at the heart of the sea ice prediction problem. While the
73 climatological seasonal cycle and even observed trends provide an initial expectation for the sea
74 ice conditions that will be present in a particular region at a particular time of year, the
75 departures from the climatological mean, whether or not the mean is adjusted for a trend, is
76 affected by the atmospheric forcing (winds, air temperatures, radiative fluxes) and oceanic
77 forcing (currents, water temperatures) of the particular year in addition to antecedent ice
78 conditions themselves. These departures have a large component of internal variability and hence
79 are difficult to predict over monthly and seasonal timescales (Serreze et al., 2016), raising
80 questions about the extent to which sea ice variations may be predictable.

81 Fully coupled models, which determine both the atmospheric and ocean/ice conditions
82 prognostically, are now used increasingly often for seasonal sea ice predictions. Ensembles of
83 coupled simulations are generally run because of the chaotic nature of the climate system. These
84 models can be run for much longer time periods than the observational sea ice record, so they
85 can provide statistics of sea ice persistence (autocorrelations) and other atmosphere-ocean-sea
86 ice relationships subject to the “perfect model” assumption, whereby model output is treated as if
87 it were data from the real world. In other words, the model’s world is regarded as equivalent to
88 the actual climate system. Examples of studies employing the “perfect model” approach are

89 Holland et al. (2011), Blanchard-Wrigglesworth et al. (2011), Day et al. (2014), Bushuk et al.
90 (2017) and Bushuk et al. (2018). In these model simulations, autocorrelation of sea ice
91 anomalies tends to be greater in the model results than in observational data (e.g., Blanchard-
92 Wrigglesworth et al., 2011, their Fig. 2; Day et al., 2014, their Fig. 1). However, skill in perfect
93 model simulations is not due solely to persistence, as physical and dynamical processes driving
94 changes in sea ice can be captured by models.

95 The skill of persistence-based statistical forecasts of sea ice variations beyond the mean
96 seasonal cycle and on-going trends is the main focus of this paper. While various prior studies
97 (cf. Section 2) have utilized broader approaches to evaluating sea ice predictability and the skill
98 of forecasts, the present study is limited specifically to statistical predictions of regional (and
99 pan-Arctic) September sea ice extent based on auto-correlation (anomaly persistence, often
100 referred to as “memory”) and lagged cross-correlations with other sea ice coverage quantities.
101 Other approaches to sea ice predictability include the use of models, which can be initialized to
102 obtain deterministic forecasts verifiable with observations or which can be run for long periods
103 in a coupled mode to assess predictability of sea ice within the “model’s world” (irrespective of
104 observations). We also do not use atmospheric or oceanic predictors in our evaluation of
105 persistence-based predictability. Atmospheric predictors in the form of known teleconnection
106 patterns have been used in statistical studies by Drobot (2003) and Lindsay et al. (2008), while
107 Bushuk et al. (2017) concluded from a dynamical model hindcast study that ocean temperature
108 initialization contributes to skill of seasonal forecasts of sea ice in the North Atlantic subarctic
109 seas. This conclusion is consistent with Blanchard-Wrigglesworth et al.’s (2011) finding that
110 across-season persistence of ocean temperature anomalies makes a detectable contribution to
111 seasonal sea ice predictability. The present study also does not include ice thickness, which has
112 been shown to be an important source of predictive skill for summer sea ice (Day et al. 2014;
113 Collow et al. 2015; Dirkson et al. 2017; Zhang et al. 2018). Guemas et al. (2016) provide a
114 review of the various approaches to sea ice prediction and sources of predictability.

115 The present paper extends the temporal window of Drobot’s (2003) study of the
116 predictability of Beaufort-Chukchi sea ice. Drobot used data from 1979-2000 to assess
117 predictability of a measure of Beaufort Sea summer ice severity (Section 3 below) based on
118 antecedent sea ice conditions as well as several atmospheric indices. While the present study will
119 not include the type of multiple-predictor evaluation carried out by Drobot, it will provide a more

120 comprehensive and updated assessment of sea ice anomaly persistence in a predictive context.
121 Drobot (2003) found that, in predictions based on indicators from the previous seasons, the
122 limited sample of years used in developing the statistical models raises questions about broader
123 applicability. In this regard, Drobot (2003, p. 1161) states "...if the Arctic climate changes, the
124 methods described here will need to be altered". In fact, the Arctic climate and, in particular, its
125 sea ice regime, have changed with the unprecedented retreat of sea ice in the post-2000 period.
126 The impact of the trend on statistical predictability is a focus of the present paper. We note,
127 however, that evolving physical relationships that underlie trend-related changes in statistical
128 relationships are not addressed in the present study.

129 In the present paper, we use the autocorrelation statistic to quantify the skill of persistence as
130 a control forecast of pan-Arctic and regional sea ice extent. In addition to utilizing the more
131 conventional metric of ice extent in regional and pan-Arctic domains, we include a regional sea
132 ice index developed in the 1970s to capture interannual variations of marine access in the
133 Beaufort Sea. A primary focus of the evaluation is the method of detrending the data, as various
134 alternative methods have not been fully explored in the literature. We show that the piecewise
135 linear method generally results in the smallest residual variance about the trend line, and we then
136 perform an across-region synthesis of information on the break-points of the two-piece linear
137 trend lines in different seasons. Our period of analysis extends back to 1953, which results in a
138 considerably larger sample of years than the more commonly used satellite period (1979
139 onward). Finally, we examine lagged cross-correlations to determine whether pan-Arctic ice
140 extent or Beaufort Sea summer ice conditions are foreshadowed in a statistical sense by
141 antecedent ice conditions in particular subregions of the Arctic.

142 More generally, the results presented here can serve to provide a baseline for distinguishing
143 contributions to seasonal sea ice forecast skill arising from climatological sea ice coverage, sea
144 ice persistence, and sea ice trend. This baseline can, in turn, serve as benchmarks for measuring
145 improvements achieved by more sophisticated prediction approaches such as dynamical models,
146 analog systems, neural networks and other more comprehensive statistical methods. The Sea Ice
147 Outlook, coordinated by the Sea Ice Prediction Network now in its Phase 2
148 (<https://www.arcus.org/sipn/sea-ice-outlook>, accessed 11 February 2019), provides an annual
149 compilation of seasonal sea ice forecasts, which are grouped into three categories:
150 physical/dynamical models, statistical methods, and heuristic approaches. While the

151 methodology used in this paper falls into the statistical category, the distinctions between (a)
152 pan-Arctic and regional skill and (b) trend-derived and interannual forecast skill are relevant to
153 all three approaches to sea ice prediction.

154

155 **2. Previous work**

156 Baselines for persistence-based predictions have been established in previous studies
157 (e.g., Blanchard-Wrigglesworth et al., 2011; Day et al., 2014; Bushuk et al., 2017, 2018). While
158 these studies generally used long control runs from climate models, their observational records
159 were limited to the post-1979 period of satellite data. The present study is based on a longer
160 observational record (back to 1953 rather than 1979). The main intent of the paper is to show
161 how detrending is a key step in the depiction of persistence-based statistical predictions. We
162 illustrate the effect of detrending for both pan-Arctic ice extent and regional metrics in order to
163 show that predictive applications on both scales must address detrending in a rigorous way, and
164 that there are various alternatives for detrending. While these alternative detrending strategies
165 are known, the relative effectiveness of the various alternatives has not been addressed in
166 previous studies. Goldstein et al. (2016; 2018) come closest by comparing representations based
167 on linear trends and discontinuities in the mean. An additional novel outcome of the present
168 study is the synthesis of break-point information.

169 The extension back to 1953 is especially noteworthy because of the recent reduction of
170 Arctic sea ice coverage has occurred almost entirely in the post-1978 period of satellite coverage.
171 On both pan-Arctic and regional scales, ice extent was relatively stable during the 1950s, 1960s
172 and 1970s, although interannual variations were then, too, a prominent feature of the time series
173 (Walsh et al., 2016). While Drobot (2003) and Lindsay et al. (2008) made use of sea ice data
174 extending back to the 1950s, there has been no systematic comparison of sea ice anomaly
175 persistence during the satellite era with anomaly persistence over longer time periods.

176 **3. Metrics of sea ice coverage**

177 Historical variations of sea ice are documented using various metrics, including pan-Arctic
178 sea ice extent, ice-covered area, and thickness. Sea ice extent is the total area within the ice
179 edge, which is typically taken to be the 15% contour of sea ice concentration. Ice extent is

180 readily obtainable from satellite measurements, as is the actual ice-covered area if the open water
181 within the ice edge is accurately depicted. Surface-based observations from ships or coastal
182 locations typically capture only the ice edge and are therefore useful primarily in the mapping of
183 ice extent. While digitized records of ice extent reaching back to the 1800s exist, there are no
184 such historical products for ice thickness. *In situ* measurements of ice thickness are sparse in
185 space and time, as are submarine sonar measurements, which are not only sparse but often
186 remain unavailable. Holt (2018) provides a rare compilation of *in situ* measurements. Satellite-
187 derived estimates of ice thickness are subject to considerable uncertainty and have only recently
188 come into use (e.g., Lindsay and Schweiger 2015), while dynamic-thermodynamic model-based
189 reconstructions of historical sea ice thickness variations have only recently been attempted
190 (Schweiger et al., 2019).

191 To explore the statistical skill that may be inherent in the spatial distribution of sea ice, we
192 compute ice extent using the gridded Arctic-wide sea ice concentration product known as
193 “Gridded Monthly Sea Ice Extent and Concentration, 1850 Onward (Walsh et al., 2015), referred
194 to in the National Snow and Ice Data Center (NSIDC) catalog as G10010. This dataset is based
195 on observations from approximately 15 historical sources between 1850 and 1978: the earliest
196 are whaling records, and the most complete, in terms of coverage, are the Arctic-wide analyses
197 that what is now the U.S. National Ice Center began in the early 1970s. Beginning in 1979, sea
198 ice concentrations from passive microwave data are used exclusively in G10010. Ice
199 concentration fields on the 15th of each month were taken from the *NOAA/NSIDC Climate Data*
200 *Record of Passive Microwave Sea Ice Concentration, Version 2* (Meier et al., 2013).

201 Prior to the 1950s, most observations were from near or just within the ice edge. If only the
202 ice edge position was known, a gradient of ice concentration within the edge was imposed in
203 order to integrate the observations into G10010. The gradient was based on a climatology
204 constructed from the passive microwave data. Spatial and temporal gaps in observations were
205 filled using an analog technique that is described in the data product documentation. Each
206 month’s sea ice concentration field in G10010 is an estimate of conditions at one time in the
207 month, nominally the 15th day of the month (or as close to the 15th as data were available). The
208 fields are at quarter-degree resolution. From these fields one can derive monthly sea ice extent
209 values. Sea ice extent is computed as the area, in sq km, covered by all cells that contain ice in

210 any concentration greater than 15%. Sea ice extent is always greater than or equal to the actual
211 ice-covered area, which excludes the area of open water within the main ice pack.

212 Various studies (e.g. Partington et al., 2003; Agnew and Howell 2002) have shown that
213 passive microwave-derived sea ice data tend to underestimate ice concentration when compared
214 with operational analyses. The *Climate Data Record of Passive Microwave Sea Ice*
215 *Concentration* is a blend of output from two algorithms that results in higher ice concentrations
216 overall for a better match with the operational analyses that predate the satellite record. Even
217 so, one might expect to see a discontinuity in the G10010 time series of ice extent when the
218 passive microwave record starts in 1979, but this is not evident (see Fig. 10 in Walsh et al.,
219 2016). While G10010 gives a record of ice extent that has realistic variability back to 1850, it is
220 difficult to assign an uncertainty to the concentration fields and ice extent values derived from
221 them. Ice extent will be more accurate than actual ice-covered area because there are many more
222 observations of the ice edge than of the concentrations within interior pack. For this reason, we
223 base our analysis on ice extent. It should be noted, however, that persistence time-scales of pan-
224 Arctic sea ice area have been shown in previous studies (e.g., Blanchard-Wrigglesworth et al.,
225 2011) to be longer than those of pan-Arctic sea ice extent because high-frequency forcing can
226 change ice extent more than it changes ice area (i.e., by converging or diverging ice floes in the
227 absence of ridging or melt).

228 G10010 was used to compute the time series of monthly sea ice extent for the pan-Arctic
229 domain and various Arctic subregions in which sea ice is at least a seasonal feature. The
230 regionalization adopted here follows that of the MASIE (Multisensor Analyzed Sea Ice Extent)
231 product available from the National Snow and Ice Data Center
232 (http://nsidc.org/data/masie/browse_regions, accessed 27 Dec 2018). MASIE (NIC and NSIDC,
233 2010) regions are defined by the U.S. Navy-NOAA-Coast Guard National Ice Center (NIC) on
234 the basis of operational analyses areas. We use the following MASIE regions: (1) Beaufort Sea,
235 (2) Chukchi Sea, (3) East Siberian Sea, (4) Laptev Sea, (5) Kara Sea, (6) Barents Sea, (7) East
236 Greenland Sea, (8) Baffin Bay/Davis Strait, (9) Canadian Archipelago, (10) Hudson Bay, (11)
237 central Arctic Ocean and (12) Bering Sea. There are several other MASIE regions (Baltic Sea,
238 Yellow Sea, Cook Inlet) that are not used here because they are not geographically connected
239 with the main Arctic sea ice cover. Figure 1 shows the regions.

240 We also make use of the long ice extent record provided by G10010 to investigate the extent
241 to which the Barnett Severity Index, or BSI, may be statistically predictable from antecedent ice
242 extent. The BSI is directly relevant to offshore navigation applications in the Beaufort Sea. It is
243 a metric of the severity of ice conditions, such as conditions encountered by barges resupplying
244 the North Slope. The BSI is determined once per year, at the end of the summer shipping season,
245 by analysts at the NIC. It is a unit-less linear combination of five parameters: 1) the distance in
246 nautical miles from Point Barrow northward to the ice edge on 15 September, 2) the distance
247 from Point Barrow northward to the 4/8th ice concentration line on 15 September, 3) the number
248 of days the entire sea route from the Bering Strait to Prudhoe Bay is ice-free in a calendar year,
249 4) the number of days the entire sea route to Prudhoe Bay is less than or equal to 4/8th ice
250 concentration in a calendar year, and 5) the temporal length of the navigable season, defined as
251 the time period from the initial date the entire sea route is less than 4/8th ice concentration to 1
252 October (Barnett, 1980). Figure 2 is a time series of the BSI reconstructed from gridded sea ice
253 concentration data (see Appendix). Higher values indicate less severe ice conditions.

254 **4 Methods**

255 As shown in Figure 3, Arctic sea ice extents have generally been decreasing over the post-
256 1953 period of this study. The Beaufort Sea is a prime example of a region in which summer
257 and autumn sea ice coverage has been decreasing, although winter (March) sea ice extent in the
258 Beaufort Sea shows no trend or variability because the ice edge extends to the coastline in March
259 of every year, essentially eliminating year-to-year variations. Consistent with the September
260 decrease of Beaufort ice extent, the BSI has been increasing over the past few decades (Figure
261 2). Two time series containing trends over time can show a correlation simply because the trends
262 are present in the time series. A trend can be used as a predictive tool by assuming its
263 continuation into the future. However, a trend can inflate persistence-based forecast skill when a
264 variable is used to predict itself (assuming the historical trend continues into the future). Indeed,
265 depictions of time-variations of a quantity such as sea ice extent are often shown as departures
266 from a trend line in order to highlight the interannual variations. One of our main interests in this
267 study is whether or not interannual variations of preceding regional ice extents correlate with
268 later BSI values. In order to exclude the effect of the overall trends in the correlation of these
269 time series, we detrend the data and explore various methods for doing so.

270 The choice of a function with which to de-trend the time series should be determined by
271 features of the series itself. The detrended time series should exclude the general tendency to
272 change over time, but preserve a measure of the year-to-year variability of the series. The
273 previous studies cited in Section 2 (e.g., Blanchard-Wrigglesworth et al., 2011; Sigmund et al.,
274 2013; Day et al., 2014; Bushuk et al., 2017, 2017) have generally relied on least-squares linear
275 fits, while Dirkson et al. (2017) suggested the use of a quadratic fit for detrending pan-Arctic sea
276 ice area.. Goldstein et al. (2016, 2018), by contrast, showed that discontinuous changes in the
277 mean better captured time series (such as open water area) characterized by abrupt changes. In
278 the spirit of the Goldstein et al. studies, we explore various options for detrending a time series
279 such as those in Figures 2 and 3, for which the changes are more pronounced in recent decades
280 than in earlier decades. In such cases, a single multi-decadal trend line cannot be expected to
281 optimally represent the historical evolution.

282 We explored several functional forms that fit the time series, including linear, quadratic,
283 cubic, and exponential functions. We found that a simple two-piece linear function – wherein
284 the data are modelled by two line segments that intersect at a ‘break-point’ year – had the lowest
285 average RMS difference between the time series and the fitted function, although fits using other
286 functions had only slightly larger RMS differences. This choice of the detrending fit has the
287 additional feature of giving a sense of when the ice extent began to change more rapidly.

288 The two-piece linear fits were obtained by using standard statistical algorithms. A
289 function defined by two intersecting half-lines can be specified by the coordinates of one point
290 on each half-line and the intersection point. With the x-axis as time, and the y-axis as the value
291 of the sea ice extent, the x-values of the non-intersecting points can be chosen to be 1953 and
292 2013, the first and last years of the BSI dataset. This leaves four values for the function to fit:
293 the series value in 1953, the series value in 2013, and the year and value at the intersection point,
294 also referred to here as the break-point. We note that the break-point is not specified by the user
295 but is determined by the algorithm so that the fit to the time series is optimized. The “curve_fit”
296 method is defined in lines 504-794 of the file
297 <https://github.com/scipy/scipy/blob/master/scipy/optimize/minpack.py> This method performs a
298 least-squares fit to the function by modifying the equation's parameters. A starting "guess" of the
299 equation parameters is provided by the user. The 'curve_fit' method of the SciPy numerical

300 library are then used to algorithmically modify the equation parameters to find the best two-piece
301 linear fit to the function.

302 In Figure 4, we show the piecewise linear fit together with quadratic, cubic and exponential
303 fits to the time series of the BSI and the September Beaufort Sea ice extent. In the case of the
304 two-piece linear fit, the break-point -- found by the `curve_fit` procedure to best fit the data -- is in
305 the early 1990s for both sea ice metrics. It is visually apparent from Figure 4 that all four fits are
306 comparable in terms of the overall magnitudes of the departures from the trend lines. The root-
307 mean-square departures from the various trend lines indeed differed by less than 10%. Because
308 the two-piece linear fit was usually the best fit and also provided a clear estimate -- the break-
309 point year -- of when the recent rate of sea ice loss accelerated, we chose the two-piece linear for
310 the remainder of this study. The break-points are computed separately for each region allowing
311 the use of the two-piece linear fit to compare the timing of the change in ice loss rate among the
312 various subregions.

313 After using the `'curve_fit'` method to find two-piece linear fits to the BSI and the regional
314 and pan-Arctic sea ice extent time series, we subtracted this linear fit from the original data to get
315 a detrended time series for each sequence. We were then able to use the `'linregress'` method
316 from the SciPy (Jones et al., 2001) software library to find the linear relationship between the
317 detrended regional monthly extent values and both the detrended BSI and the detrended pan-
318 Arctic extent. We then used the `'stats'` method from SciPy to compute the square of the Pearson
319 correlation coefficient (R^2) and the p-value estimate of statistical significance for this
320 relationship.

321

322 **5 Results**

323 As noted in Section 2, previous studies (Bushuk et al., 2018) have evaluated the persistence
324 of regional ice extent over the post-1978 period of satellite observations. Here we extend this
325 evaluation to encompass a longer period dating back to 1953 in order to assess the stability of the
326 persistence statistics. Specifically, for each region in Figure 1, we have correlated the September
327 ice extent with the ice extent of antecedent months for the 1953-2013 and 1979-2013 periods.
328 Figure 5 compares these persistence values (autocorrelations at multimonth lags), for the
329 antecedent months of March, May and July in a subset of regions. Because the regions chosen
330 were those that have interannually varying ice cover in September, regions such as the Bering

331 Sea, Hudson Bay, the Sea of Okhotsk and the Baltic Sea were excluded. The correlations for the
332 non-detrended and detrended ice extents are shown in panels (a) and (b), respectively.

333 For most of the regions, the inclusion of the earlier decades does not have a notable impact
334 on the persistence from July to September, and detrending the data does not change this
335 conclusion. However, in the non-detrended results of Figure 5a, the March-to-September and
336 May-to-September correlations change substantially in a few regions. The Baffin Bay March-to-
337 September correlations increase from 0.00 to 0.34 when the earlier decades are eliminated,
338 largely as a result of the post-1979 trend: the post-1979 correlation is statistically significant ($p <$
339 0.05) based on a Wald test with t-distribution of the test statistic and a two-sided p-value for a
340 null hypothesis that the slope is zero. The pan-Arctic correlations, as Figure 5a shows, are
341 higher than the correlations for the individual regions, also increase when the earlier decades are
342 eliminated. In the Greenland Sea, the correlations from March and May decrease substantially
343 and lose statistical significance when the earlier decades are eliminated.

344 As shown in Figure 5b, the detrending generally reduces the magnitudes of the
345 correlations between September and the earlier months, both for the longer post-1953 periods
346 and the shorter post-1979 periods: The March-to-September correlations based on the detrended
347 data for the longer/shorter periods are: -0.05/0.20 for Baffin Bay, 0.20/0.13 for the Barents Sea,
348 0.00/0.00 for the Beaufort Sea (no March variance), 0.00/0.00 for the Canadian Archipelago (no
349 March variance), -0.15/0.00 for the Chukchi Sea, 0.07/0.21 for the East Siberian Sea, 0.25/-0.03
350 for the Greenland Sea, 0.03/0.03 for the Kara Sea, and 0.07/0.18 for the Laptev Sea. The
351 corresponding 5% significant levels are 0.26/0.33. Except for the Canadian Archipelago and
352 East Siberian regions, the May-to-September correlations in Figure 5b are also small (<0.40).
353 Only the July-to-September correlations are above 0.40 in all regions for the detrended data. In
354 view of generally small magnitudes of the March-September and May-September correlations in
355 Figure 5b, we conclude that the springtime “predictability barrier” (Lindsay et al., 2008; Day et
356 al., 2014; Bushuk et al., 2018) in regional forecasts based on persistence of ice extent anomalies
357 is not reduced by the inclusion of several decades of pre-satellite data.

358 Because changes of trend have not been addressed systematically in previous evaluations of
359 Arctic sea ice trends, we synthesized the break-point information across all regions and calendar
360 months (January-September) included in our study. The synthesis was limited to only those
361 regions and calendar months in which the two-piece linear fit reduced the root-mean-square

362 residual by at least 5% relative to the one-piece linear best fit. Figure 6 groups the break-points
363 into five year periods ending in 1955, 1960,..., 2015. In order to capture the seasonality of the
364 break-points, we present separate plots for (a) the entire January-September period, (b) January-
365 March (winter), (c) April-June (spring), and July-September (summer). As shown in panel ((a),
366 nearly all the break-points occur in the second half of the study period, with a maximum in 1991-
367 1995. The 1991-1995 period has the most break points of any 5-year period, and the 1990s have
368 nearly as many break points as all the other decades combined. The small secondary peak in the
369 1960s represents eight break-points scattered across the regions and seasons (Cook Inlet in
370 January and February; East Siberian Sea in February and April; pan-Arctic in July; Hudson Bay
371 in August; Baffin-St. Lawrence and Bering in September), showing no systematic pattern that
372 would suggest a meaningful signal. The winter and summer seasons are the primary contributors
373 to the maximum in the 1990s, as the spring break points are evenly distributed through the latter
374 half of the study period. However, spring has the fewest (12) break-points overall, while the
375 summer has the most (26). The break-points for our focal metrics, the BSI and September pan-
376 Arctic ice extent, are 1991 and 199, respectively, consistent with the distribution in Figure 6.
377 These two metrics are included in the results summarized in Figure 6. One may conclude that
378 the 1990s, and to a lesser early 2000s, represent the shift to a more rapid rate of sea ice loss. If
379 one is to argue for a “regime shift” in Arctic sea ice loss (Lenton, 2012), this period would be the
380 leading candidate.

381 In order to illustrate the effect of the detrending and to show which regions contribute the
382 most explained variance to pan-Arctic sea ice extent, Figure 7 shows the squares of the
383 correlations (R^2) between September pan-Arctic ice extent and the concurrent ice extent in each
384 of the subregions. The figure shows values of R^2 before detrending (upper numbers, regular
385 font) and after detrending (lower numbers, bold font). With the trend included, the R^2 values are
386 relatively high in most regions (except for the Bering Sea), ranging from 0.32 to 0.71; the
387 corresponding correlations (R) range from 0.57 to 0.84. Based on the t-test described earlier,
388 these correlations all exceed the 95% significance thresholds, which range from 0.26 ($R^2 = 0.07$)
389 for a 60-year sample with no autocorrelation to 0.38 ($R^2 = 0.14$) for a 60-year sample with an
390 autocorrelation of 0.4. None of the regional or pan-Arctic ice extent autocorrelations exceeded
391 0.40. Because these correlations are dominated by the trend, the larger values appear in the
392 regions with trends that are most similar to the pan-Arctic trend. When the data are detrended,

393 the explained variances are much smaller (R^2 values in bold font in Figure 7) although still larger
394 than the 95% significance thresholds for a 60-year sample ($R = 0.26$, $R^2 = 0.07$). These smaller
395 values indicate the relative contributions of regional variations to the interannual variations of
396 pan-Arctic ice extent. According to Figure 7, the regions contributing most strongly to
397 September pan-Arctic sea ice variations (including trends) are the Beaufort, Chukchi and East
398 Siberian Seas. After the data are detrended, the regions contributing most to September pan-
399 Arctic sea ice variations are the East Siberian and Laptev Seas. The relatively large contribution
400 of the Laptev Sea is consistent with the “dynamical preconditioning” hypothesis of Williams et
401 al. (2016). The variances of the detrended pan-Arctic September extents explained by the East
402 Siberian and Laptev Seas are indeed among the largest of all the regions, although the Chukchi
403 Sea’s interannual variance is essentially as large.

404 Figure 8 shows the squares of the correlations between the annual BSI and regional
405 September ice extent before the detrending of both variables (top numbers) and after detrending
406 (bottom numbers). While the actual correlations between the BSI and regional extent are
407 generally negative, the R^2 values plotted in Figure 8 are positive. Large values of R^2 appear in
408 most regions when the trend is included (upper numbers) because the BSI has a strong positive
409 trend over time while September ice extent in most regions has a negative trend. The R^2 values
410 are much weaker in regions away from the Beaufort Sea when the trends are removed (lower
411 numbers in Fig. 8). The detrended R^2 values show the spatial representativeness of the BSI as a
412 measure of interannual variations in each region. Figure 8 shows that the regions of significant
413 explained variance include the Canadian Archipelago to the east as well as the Chukchi Sea to
414 the west. However, the “scale of influence”, if measured by the area of significant correlation, is
415 smaller for the BSI in Fig. 8 than for pan-Arctic ice extent in Fig. 7.

416 Because the potential for seasonal predictions is a key motivation for this study, we
417 examine cross-correlations in which the predictands (pan-Arctic ice extent and the BSI) lag
418 potential predictors (regional ice extents) by intervals ranging from zero (no lag) to several
419 seasons. Cross-correlations between non-detrended and detrended September pan-Arctic and
420 regional ice extents are summarized in Tables 1 and 2 respectively. Cross-correlations between
421 non-detrended and detrended BSI and regional ice extent are given in Tables S1 and S2
422 respectively. In all cases, the numerical values are the R^2 values. In order to illustrate the
423 contribution of the trend to the apparent forecast skill, we present these correlations graphically

424 for the regions which show the strongest associations with the September predictands. Figure 9
425 shows the R^2 values for cases in which September pan-Arctic ice extent lags by 0, 1, 2, ..., 8
426 months the ice extent in five subregions: the Beaufort, Chukchi, East Siberian, Barents and
427 Laptev Seas. The red bars correspond to correlations computed from the data with the trends
428 included. Not surprisingly, the R^2 values are largest at zero lag. The rates at which the
429 correlations decrease with increasing lag vary regionally, reaching zero by 3-4 months for the
430 Beaufort, Chukchi, and East Siberian Seas. The zero-month lag values are quite large for the
431 Beaufort, Chukchi, and East Siberian regions, where they exceed $R^2 = 0.7$ ($R = 0.84$).

432 However, after detrending (using the two-piece linear best fits), most of the apparent forecast
433 skill is lost. As shown by the blue bars in Figure 9, nearly all the predictability from the Barents
434 and Chukchi Seas vanishes with the detrending, while only small fractions of explained variance
435 remain at non-zero lags when sea ice extents for the Beaufort and East Siberian Seas are the
436 predictors. For example, when the regional extent leads by two months (July), the fractions of
437 explained variance are approximately 0.16 and 0.10 ($R \sim 0.40$ and 0.32) for the East Siberian and
438 Beaufort Seas, respectively. The implication is that the persistence of interannual variations about
439 the trend line makes only small contributions to interannual variations of pan-Arctic sea ice extent,
440 and that these small contributions result mainly from the Pacific sector of the Arctic. As indicated
441 by Figure 9, the pan-Arctic extent of July and August correlates more highly than any regional
442 extent with September pan-Arctic ice extent in both the non-detrended and the detrended data (see
443 also Tables 1 and 2).

444 The lagged R^2 values relevant to predictions of the Barnett Severity Index are shown in
445 Figure 10. Because the BSI is based primarily on ice conditions in the Beaufort Sea in August
446 and September, it is not surprising that the correlation is largest for the Beaufort's ice extent in
447 September, when the R^2 value is approximately 0.8 for data that are not detrended. The August
448 and September values for the Chukchi are essentially as large as the corresponding Beaufort
449 values, indicating a spatial coherence of the variations (with trends included) in the two regions.
450 The antecedent extents in the East Siberian and Barents regions also explain statistically
451 significant fractions of the variance when the trends are included.

452 The blue bars in Figure 10 are the lagged R^2 values based on the detrended data. Because the
453 trend's contribution to the forecast skill has been removed, these correlations provide the most
454 meaningful assessment of the seasonal forecast skill if the BSI based on antecedent ice

455 conditions. The largest correlations are for the Beaufort Sea, where the explained variances
456 decrease from about 0.55 ($R \sim 0.74$) in September to about 0.10 ($R \sim 0.32$) in June. The
457 correlations for the Chukchi are only slightly smaller, but the BSI variance explained by all other
458 regions is less than 10%. The percentage of variance explained by the antecedent ice extent of
459 the nearby regions (Beaufort, Chukchi, East Siberian Seas) is less than one might have
460 anticipated, given that the BSI includes information on the length of the navigation season,
461 which can begin well before September, i.e., as early as July in some years.

462 While the results presented here imply that the persistence of detrended sea ice anomalies
463 provide only limited forecast skill, a key question is: How much better are sea ice forecasts based
464 on other approaches? The Sea Ice Prediction Network's Sea Ice Outlook (SIO) consists of
465 seasonal forecasts of September sea extent based on a variety of approaches (numerical
466 modelling, statistical and heuristic) on an annual basis beginning in 2008. In most years, several
467 dozen individual (or groups) provide the SIO with September sea ice extent predictions based
468 data and other information available at the end of May, June and July. A compilation of SIO
469 results from 2008-2018 enables a quantitative comparison of the skill of the SIO and persistence-
470 based forecasts. (In this case, persistence was evaluated from the mean ice extents in the
471 National Snow and Ice Data Center's G02135_v3.0:
472 ftp://sidads.colorado.edu/DATASETS/NOAA/G02135/seaice_analysis/, accessed 27 Dec 2018).
473 The median absolute error of the all-forecaster average SIO issued in July of 2008-2018 is 0.32
474 million km², while the corresponding median absolute error of forecasts of persistence of the
475 departure from the trend line of the pan-Arctic ice extents of May, June, July and August are
476 0.43, 0.22, 0.25, and 0.09 million km². Thus the SIO forecasts issued in July outperform the
477 trend-line anomaly persistence forecasts from May, but not from June, July or August.
478 Persistence of the previous September's deviation from the trend line has a median absolute 0.37
479 million km², while simple persistence of the previous year's actual value has an error of 0.40
480 million km². The corresponding root-mean-square errors (in millions km²) are 0.57 for SIPN;
481 0.67, 0.46, 0.42, and 0.18 for persistence of the trend-line departures of May, June, July and
482 August; 0.68 for persistence of the trend-line departure from the previous September; and 0.67
483 for persistence of the actual extent from the preceding September. The SIO forecasts used in this
484 comparison were averages of all forecasts submitted to SIO, so it is quite possible that some
485 individual forecasters participating in the SIO perform considerably better. Nevertheless, it is

486 apparent that sea ice anomaly persistence is a challenging control forecast and a respectable
487 competitor for forecasts issued by the scientific community

488

489 **6 Conclusion**

490 The substantial decrease of Arctic sea ice over the past several decades is well documented
491 (Cavalieri and Parkinson, 2012; Parkinson, 2014; Onarheim et al., 2018). Of all the regions
492 considered here, only the Bering Sea does not show a negative trend, and the Bering trend is
493 positive only in January-April (Onarheim et al., 2018, their Table 1). Moreover, the extreme
494 minima of Bering Sea ice during the past two winters (2016-17 and 2017-18) are starting to bring
495 the Bering's trend into alignment with the other regions of the Arctic.

496 The prominence of the trends in the time series of regional as well as pan-Arctic ice extent
497 makes it important to distinguish the contribution of the trend from other sources of forecast
498 skill. In this study we explored the use of several methods of detrending in order to evaluate the
499 use of ice anomaly persistence (autocorrelation) and regional cross-correlations as predictors of
500 ice variations. The two-piece linear trend evaluations generally have break-points in the 1990s,
501 indicating that the rate of ice loss has been greater in the past two decades than in the earlier
502 portion of the satellite era that began in 1979.

503 Based on the raw (not detrended) time series, the antecedent ice extents in a substantial
504 fraction of the Arctic regional seas explain statistically significant fractions of variance of
505 September pan-Arctic ice extent and also of the Barnett Severity Index, which is more specific to
506 the Beaufort Sea. Statistically significant portions of variance of both September metrics are
507 explained by the regional ice extents of prior seasons. However, this predictive "skill" is
508 attributable primarily to the trends in the data. Removal of the trend leaves little forecast skill
509 beyond a month or two when the forecast method is limited to the relatively simple statistical
510 correlations utilized here. The low persistence-derived skill for the detrended September pan-
511 Arctic ice extent is consistent with the findings of Stroeve et al. (2014) based on the Sea Ice
512 Outlook as part of the Study of Environmental Arctic Change (SEARCH). Moreover, our
513 inclusion of data back to the early 1950s shows that the springtime "predictability barrier" in
514 regional forecasts based on persistence of ice extent anomalies is not reduced by the inclusion of
515 several decades of pre-satellite data.

516 It must be noted that other sea ice prediction approaches have outperformed persistence
517 (e.g., Tivy et al., 2007; Shröder et al., 2014; Yuan et al., 2016; Petty et al., 2017; and Bushuk et
518 al., 2018). Some of these studies have used statistical methods informed by other predictors
519 (e.g., Lindsay et al., 2008; Tivy et al., 2011), some have used the perfect model approach (e.g.,
520 Blanchard-Wrigglesworth et al., 2011), and some have made use of initialized hindcasts (e.g.,
521 Bushuk et al., 2018). Nevertheless, persistence derived skill provides a baseline for the
522 measurement of forecast skill achieved by these other approaches and, based on the results in
523 Section 5, persistence of departures from the trend line can be a challenging competitor at
524 forecast ranges of months to seasons.

525 While the variance explained by simple anomaly persistence at lead times of several seasons
526 and also by persistence of detrended anomalies at lead times of a month or two is statistically
527 significant, statistical significance does not equate to usefulness. Potential users of sea ice
528 forecasts include local communities engaging in offshore subsistence and travel activities,
529 marine transport companies, offshore resource extraction, and the tourism industry. The
530 relatively small fractions of variance predictable several months in advance using detrended data
531 (Figures 6-9) will likely leave uncertainties that are too great for many users. However the
532 trend-derived skill, which can represent 50% or more of the variance, may enable decisions if the
533 interannual variations superimposed on the trend represent acceptable risks for users of sea ice
534 forecasts.

535

536 **Acknowledgments**

537 Funding for this work was provided by the Climate Program Office of the National Oceanic and
538 Atmospheric Administration through Grants NA16OAR4310162 and by the National Science
539 Foundation through Grant OPP-1749081. Florence Fetterer was supported by the CIRES/NOAA
540 Cooperative Agreement, NOAA Grant NA15OAR4320137. We thank the two reviewers for
541 their many comments and suggestions, which have led to a more rigorous presentation. We also
542 thank Larry Hamilton of the University of New Hampshire for initiating the comparison of the
543 skill of the persistence-based forecasts and the Sea Ice Outlook.

544

545 **References**

- 546 Agnew, T. A., and Howell, S.: Comparison of digitized Canadian ice charts and passive
547 microwave sea-ice concentrations. Geoscience and Remote Sensing Symposium, 2002. IGARSS
548 '02. 2002 IEEE International 1: 231- 233. doi: 10.1109/IGARSS.2002.1024996, 2002.
- 549 AMAP: Snow, Water, Ice and Permafrost in the Arctic: 2017 Update. Arctic Monitoring and
550 Assessment Programme, Oslo, Norway, xiv + 269 pp., 2017.
- 551 Barnett, D. G.: A long-range ice forecasting method for the north coast of Alaska. Sea Ice
552 Processes and Models, R. Pritchard, Ed., University of Washington Press, 402–409, 1980.
- 553 Blanchard-Wrigglesworth, E., Armour, K. C., and Bitz, C. M.: Persistence and inherent
554 predictability of Arctic sea ice in a GCM ensemble and observations. *J. Climate*, 24, 231-250,
555 2011.
- 556 Box, J. E., and 19 Coauthors: Key indicators of Arctic climate change, 1971-2017. *Env. Res.*
557 *Lett.*, in press, 2019.
- 558 Bushuk, M., Msadek, R., Winton, M., Vecchi, G. A., Gudgel, R., Rosati, A., and Yang, X.:
559 Skillful regional predictions of Arctic sea ice on seasonal timescales. *Geophys. Res. Lett.*, 44,
560 4953-4964, doi:10.1002/2017/GL073155, 2017.
- 561 Bushuk, M., Msadek, R., Winton, M., Vecchi, G., Yang, X., Rosati, A., and Gudgel, R.:
562 Regional Arctic sea-ice prediction: potential versus operational seasonal forecast skill. *Climate*
563 *Dynamics*, <https://doi.org/10.1007/s00382-018-4288-y>, 2018.
- 564 Cavalieri, D. J., and Parkinson, C. L.: Arctic sea ice variability and trends, 1979-2010.
565 *Cryosphere*, 6, 881-889, 2012.
- 566 Collow, T. W., Wang, W., Kumar, A., and Zhang, J.: Improving Arctic sea ice prediction using
567 PIOMAS initial sea ice thickness in a coupled ocean-atmosphere model. *Mon. Wea. Rev.*, 143,
568 4618-4630, 2015.

569 Crowley Maritime Corporation, 2002. From
570 <http://www.crowley.com/content/download/11926/80932/version/1/file/Alaska-50-Years.pdf>
571 accessed 10 May 2018.

572 Day, J. J., Tietsche, S., and Hawkins, E.: Pan-Arctic and regional sea ice predictability:
573 Initialization month dependence. *J. Climate*, 27, 4371-4390, 2014.

574 Dirkson, A., Merryfield, W. J., and Monahan, A.: Impacts of sea ice thickness initialization on
575 seasonal Arctic sea ice predictions. *J. Climate*, 30, 1001-1017, 2017.

576 Drobot, S.: Long-range statistical forecasting of ice severity in the Baaufort-Chukchi Sea.
577 *Weather and Forecasting*, 18, 1161-1176, 2003.

578 Drobot, S. D., J. A. Maslanik, and Fowler, C. F.: A long-range forecast of Arctic summer sea ice
579 minimum extent. *Geophysical Research Letters*, 33, L10501, doi:10.1029/2006/GL026216,
580 2006.

581 Goldstein, M. A., Lynch, A. H., Arbetter, T. E., and Fetterer, F.: Abrupt transitions in Arctic
582 open water area. *The Cryosphere Discussion*, doi:10.5194/tc-2016-108, 2016.

583 Goldstein, M. A., Lynch, A. H., Zsom, A., Arbetter, T., Chang, A., and Fetterer, F.: The step-like
584 evolution of Arctic open water. *Nature Scientific Reports*, 8:16902, doi:10.1038/s41598-018-
585 35064-5, 2018.

586 Guemas, V., and 12 Coauthors: A review on Arctic sea-ice predictability and prediction on
587 seasonal to decadal time-scales. *Quarterly J. Royal Meteor. Soc.*, 142, 546-561, 2016.

588 Holland, M. M., Bailey, D. A., and Vavrus, S.: Inherent sea ice predictability in the rapidly
589 changing Arctic environment of the Community Climate System Model, version 3. *Climate*
590 *Dynamics*, 36, 1239-1253, 2011.

591 Holt, B.: On-Ice Arctic Sea Ice Thickness Measurements by Auger, Core, and Electromagnetic
592 Induction, From the Fram Expedition Onward. National Snow and Ice Data Center, Boulder, CO
593 USA, doi: <https://doi.org/10.7265/N58K7785>, 2018.

594 Jones E., Oliphant, E. Peterson E. *et al.*: SciPy: Open Source Scientific Tools for Python, 2001-,
595 <http://www.scipy.org/> [Online; accessed 2018-03-29].

596 Kinnard, C., Zdanowicz, C. M., Fisher, D. A., Isaksson, E., De Vernal, A., and Thompson, L. G.:
597 Reconstructed changes in Arctic sea ice over the past 1,450 years. *Nature*, 479, 509-512, 2011.

598 Kwok, R., and Rothrock, D. A.: Decline in Arctic sea ice thickness from submarine and ICESat
599 records: 1958-2008. *Geophys. Res. Lett.*, 36, L15501, 2009.

600 Laxon, S.W., Giles, K. A., Rideout, A. L., Wingham, D. J., Willatt, R., Cullen, R., Kwok, R.,
601 Schweiger, A., Zhang, J., Haas, C., Hendricks, S., Krishfield, R., Kurtz, N., Farrell, S., and
602 Davidson, M.: CryoSat-2 estimates of Arctic sea ice thickness and volume. *Geophys. Res.*
603 *Lett.*, 40, doi: 10.1002/grl.50193, 2013.

604 Lenton, T. M.: Arctic climate tipping points. *Ambio*, 41, 10-22, 2012.

605 Lindsay, R., and Schweiger, A.: Arctic sea ice thickness loss determined using subsurface,
606 aircraft, and satellite observations. *The Cryosphere*, 9(1), 269-283, 2015.

607 Lindsay, R. W., Zhang, J., Schweiger, A. J., and Steele, M. A.: Seasonal predictions of ice extent
608 in the Arctic Ocean. *J. Geophys. Res. (Oceans)*, 113, C02023,
609 <https://doi.org/10.1029/2007/C004259>, 2008.

610 Maslanik, J., Stroeve, J., Fowler, C., and Emery, W: Distribution and trends in Arctic sea ice age
611 through spring 2011. *Geophys. Res. Lett.*, 38, L13502, doi:10.10029/2011GL047735, 2011.

612 Meier, W., Fetterer, F., Savoie, M., Mallory, S., Duerr, R., and Stroeve, J: NOAA/NSIDC
613 Climate Data Record of Passive Microwave Sea Ice Concentration, Version 2. Boulder,
614 Colorado USA. NSIDC: National Snow and Ice Data Center.
615 doi:<http://dx.doi.org/10.7265/N59P2ZTG>. (G02202), 2013.

616 National Ice Center and National Snow and Ice Data Center. Compiled by Fetterer, F., Savoie,
617 M., Helfrich, S., and Clemente-Colón,: *Multisensor Analyzed Sea Ice Extent - Northern*
618 *Hemisphere (MASIE-NH), Version 1*. Boulder, Colorado USA. NSIDC: National Snow and Ice
619 Data Center. doi: <https://doi.org/10.7265/N5GT5K3K>, (G02186), 2010 (updated daily)

620 NOAA: Arctic Report Card 2017. National Oceanic and Atmospheric Administration,
621 ftp://ftp.oar.noaa.gov/arctic/documents/ArcticReportCard_handout2017.pdf (accessed 27 Dec
622 2018)

623 Onarheim, I. H., Eldevik, T., Smedsrud, L. H., and Stroeve, J. C.: Seasonal and regional
624 manifestations of Arctic sea ice. *J. Climate*, 31, 4917-4932, doi:10.1175/JCLI-D-17-0427.1,
625 2018.

626 Parkinson, C. L.: Spatially mapped reductions in the length of the Arctic sea ice season.
627 *Geophys. Res. Lett.*, 41, 4316-4322, 2014.

628 Partington, K., Flynn, T., Lamb, D., Bertioia, C., and Dedrick, K.: Late twentieth century
629 Northern Hemisphere sea-ice record from U.S. National Ice Center ice charts. *J. Geophys. Res.*
630 108(C11): 3343. doi:10.1029/2002JC001623, 2003.

631 Petty, A. A., Schröder, D., Stroeve, J., Markus, T., Miller, J., Kurtz, N., Feltham, D., and Flocco,
632 D: Skillful spring forecasts of September Arctic sea ice extent using passive microwave sea ice
633 observations. *Earth's Future*, 5, 254-263, 2017.

634 Schröder, D., Feltham, D. L., Flocco, D., and Tsamados, M.: September Arctic sea-ice minimum
635 predicted by spring melt-pond fraction. *Nature Clim. Change*, 4(5): 353–357, 2014.

636 Schweiger, A. J., Wood, K. R., and Zhang, J.: Arctic sea ice volume variability over 1901-2010:
637 A model-based reconstruction. *J. Climate*, in review, 2019..
638

639 Serreze, M. C., and Stroeve, J.: Arctic sea ice trends, variability and implications for seasonal sea
640 ice forecasting. *Phil. Trans. Royal Society A*, 373, 20140159, 2015.

641 Serreze, M. C., Stroeve, J., Barrett, A. P., and Boisvert, L. N.: Summer atmospheric circulation
642 anomalies over the Arctic Ocean and their influences on September sea ice extent: A cautionary
643 tale. *J. Geophys. Res.-Atmospheres*, 121(19): 11,463-11,485, doi:10.1002/2016JD025161, 2016.

644 Sigmund, M., Fyfe, J. C., Flato, G. M., Kharin, V. V., and Merryfield, W. J.: Seasonal forecast
645 skill of Arctic sea ice area in a dynamical forecast system. *Geophys. Res. Lett.*, 40, 529-534,
646 doi:10.1002/grl.50129, 2013.

647 Stroeve, J., Hamilton, L. C., Bitz, C. M., and Blanchard-Wrigglesworth, E.: Predicting September
648 sea ice: Ensemble skill of the SEARCH Sea Ice Outlook, 2008-2013. *Geophys. Res. Lett.*, 41,
649 2411-2418, 2014.

650 Tivy, A., Alt, B., Howell, S. E. L., Wilson, K., and Yackel, J.: Long-range prediction of the
651 shipping season in Hudson Bay: A statistical approach. *Weather and Forecasting*, 22, 1063-1075,
652 2007.

653 Tivy, A., Howell, S. E. L., Alt, B., Yackel, J. J., and Carrieres, T.: Origins and levels of seasonal
654 forecast skill for sea ice in Hudson Bay using canonical correlation analysis. *J. Climate*, 24, 1378-
655 1394, 2011.

656 Walsh, J. E., Fetterer, F., Stewart, J. S., and Chapman, W. L.: A database for depicting sea ice
657 variations back to 1850. *Geograph. Rev.*, 107, 89-107, 2016.

658 Walsh, J. E., Chapman, W. L., and Fetterer, F.: Gridded Monthly Sea Ice Extent and
659 Concentration, 1850 Onward, Version 1. Boulder, Colorado USA. NSIDC: National Snow and
660 Ice Data Center. doi: <http://dx.doi.org/10.7265/N5833PZ5>, (G10010), 2015 (updated 2016).

661 Williams, J., Tremblay, B., Newton, R., and Allard, R.: Dynamic preconditioning of the
662 minimum September sea ice extent. *J. Climate*, 29, 5879-5891, 2016.

663 Yuan, X., Chen, D., Li, C., and Wang, W.: Arctic sea ice seasonal prediction by a linear markov
664 model. *J. Climate*, 29, 8151-8173, 2016.

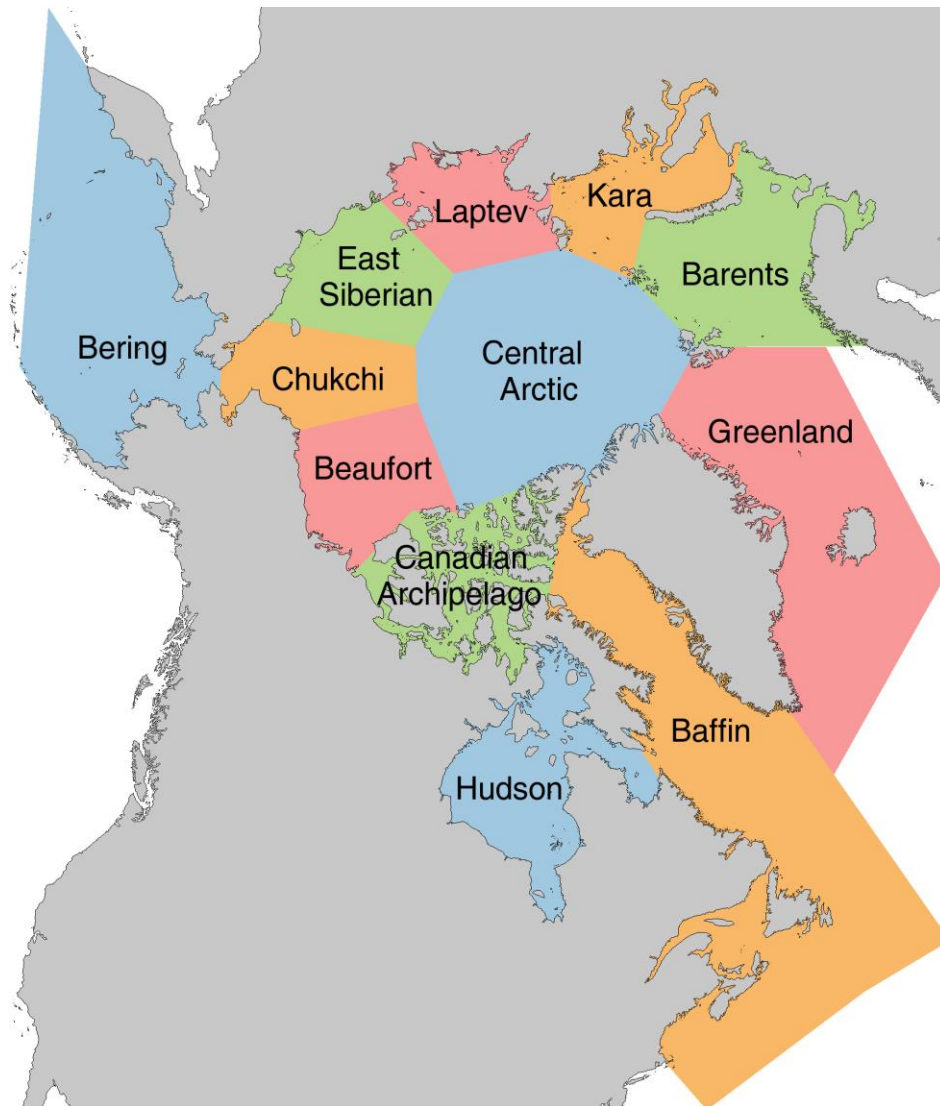
665 Zhang, Y., Bitz, C. M., Anderson, J. L., Collins, N., Hendricks, J., Hoar, T., Raeder, K., and
666 Massonnet, F.: Insights on sea ice data assimilation from perfect model observing system
667 simulation experiments. *J. Climate*, 31, 5911-5926, 2018.

668 **Appendix.** Reconstruction of the Barnett Severity Index, 1953-2013

669
670 As described in Section 2, the Barnett Severity Index (BSI) is a combination of five metrics of ice
671 coverage in the Beaufort Sea. Drobot et al. (2003) used the BSI through 2000 in their evaluation
672 of predictability based on multilinear regression against various measures of sea ice cover. In
673 order to update the BSI for use in this study, we base a reconstruction on the digital grids of sea
674 ice concentration in the Historical Sea Ice Atlas (HSIA) for Alaska (<http://seaiceatlas.snap.uaf.edu/>
675 accessed 27 Dec 2018). As with the regional ice extent calculations using G10010 (Section 3), we
676 use the HSIA because it extends the record 26 years back in time before the start of the satellite
677 passive microwave record. While the sources of the ice concentration data in the HSIA are the
678 same as in G10010, a notable advantage of the HSIA is its weekly temporal resolution (vs. the
679 monthly resolution of G10010). The HSIA also has a spatial resolution of $\frac{1}{4}^{\circ}$ latitude by $\frac{1}{4}^{\circ}$ degree
680 longitude. Because of the weekly time resolution, the distance metrics (3)-(5) of the BSI are
681 truncated to the nearest week. Similarly, the distance metrics (1) and (2) are truncated to the
682 nearest 27.8 km (15 n mi). One of the within-month dates of the HSIA grids is the 15th of each
683 month, so no temporal interpolation is necessary for metrics (1) and (2). The reconstructed values
684 of the BSI are listed in Table A1.

685

686



687
688
689
690

Figure 1. The MASIE subregions used in the study (NIC and NSIDC, 2010).

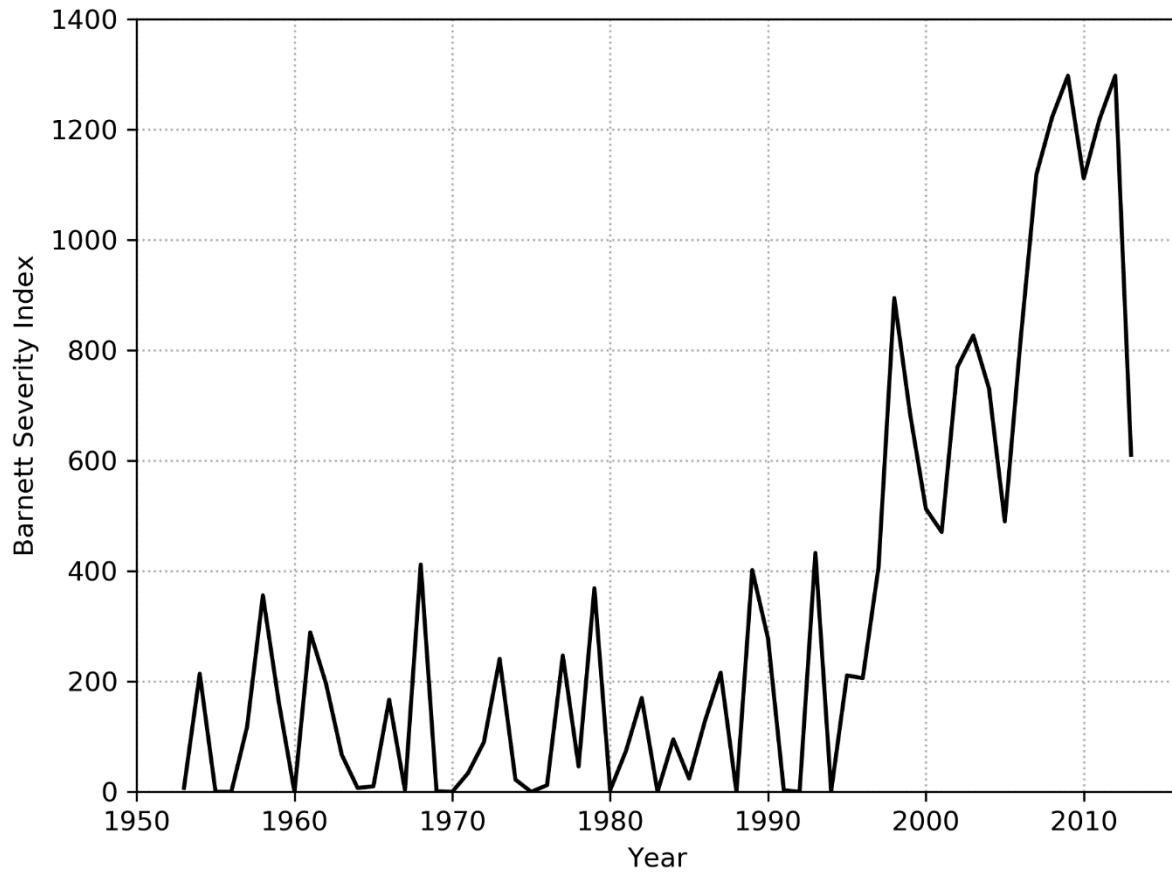
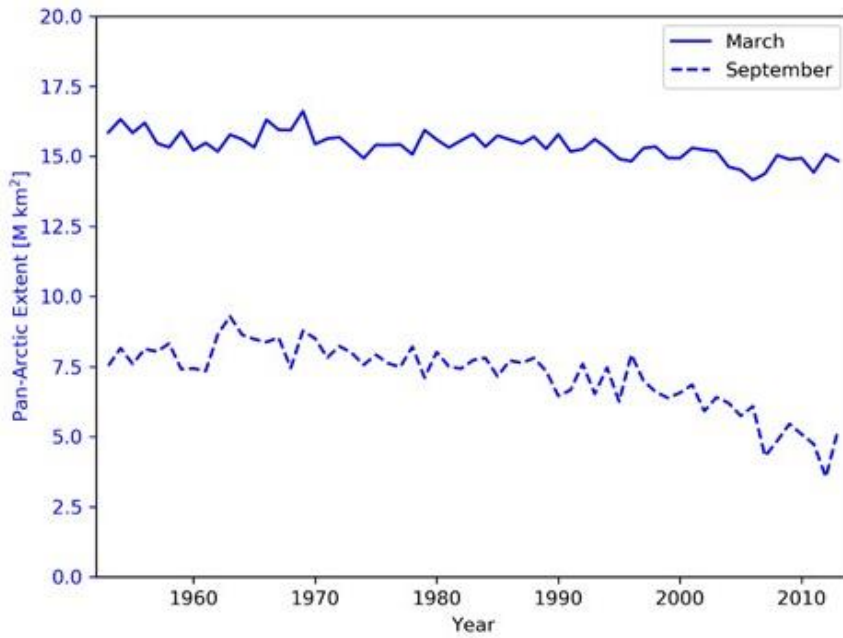
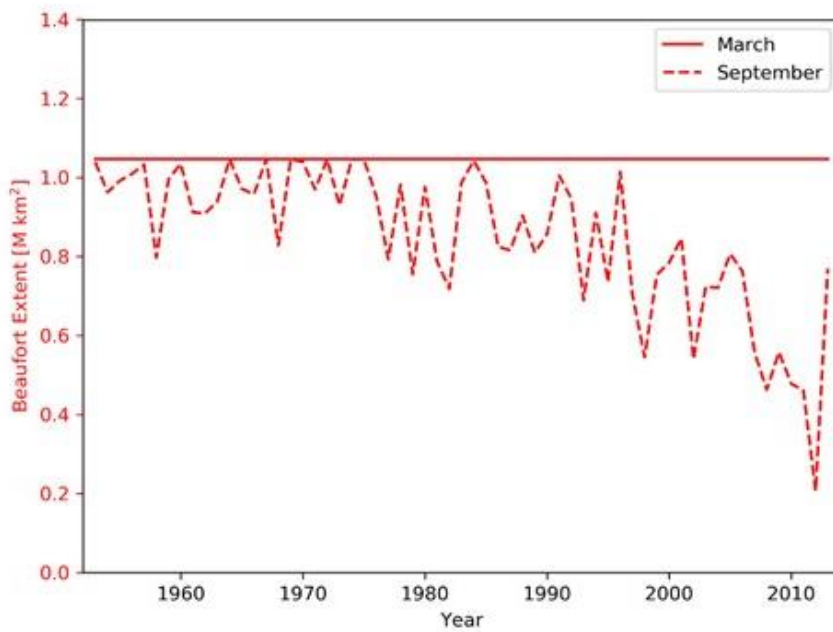


Figure 2. Time series of the Barnett Severity Index (BSI), 1953-2013.

691
 692
 693
 694
 695
 696



(a) Pan-Arctic



(b) Beaufort

697

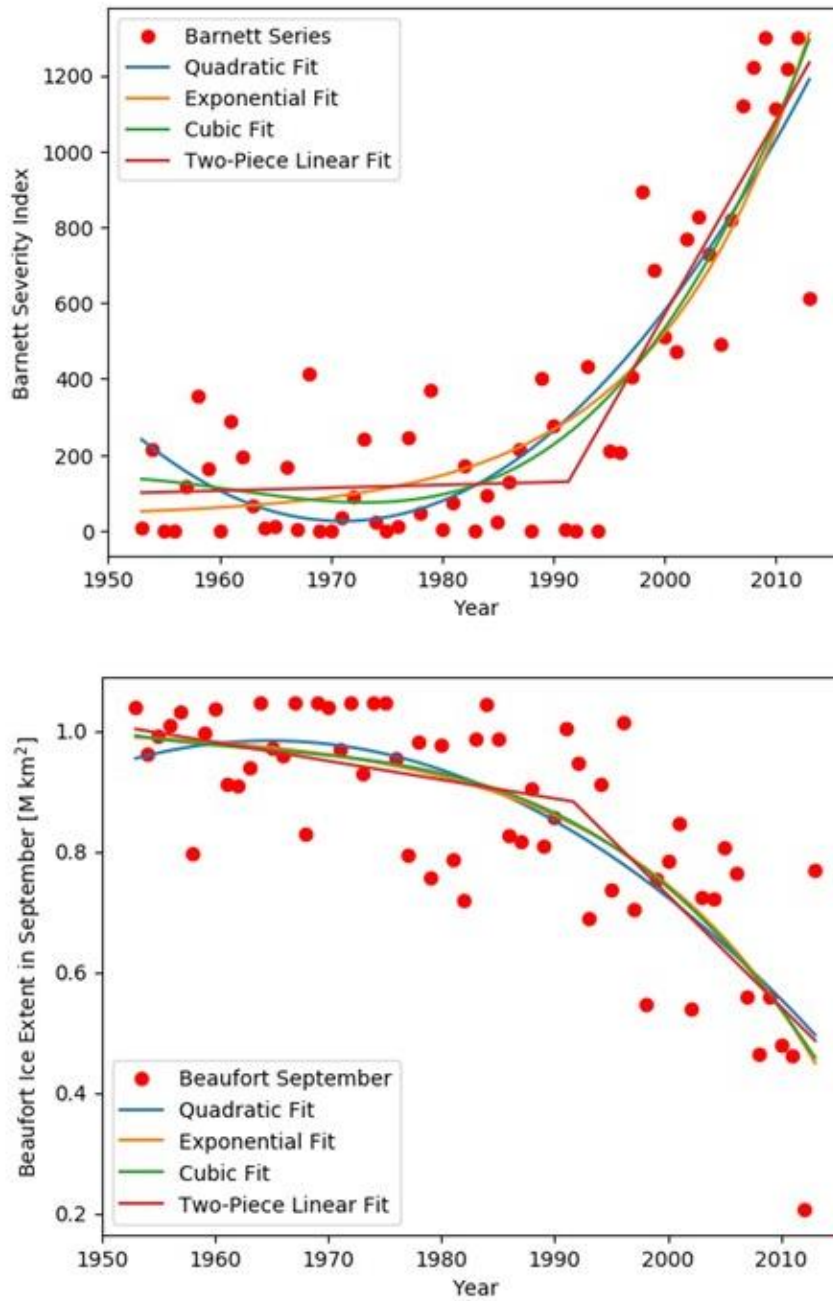
698 **Figure 3.** (a) Total Arctic sea ice extent and (b) the extent of ice in the Beaufort Sea during

699

March(solid lines) and September (dashed lines) .

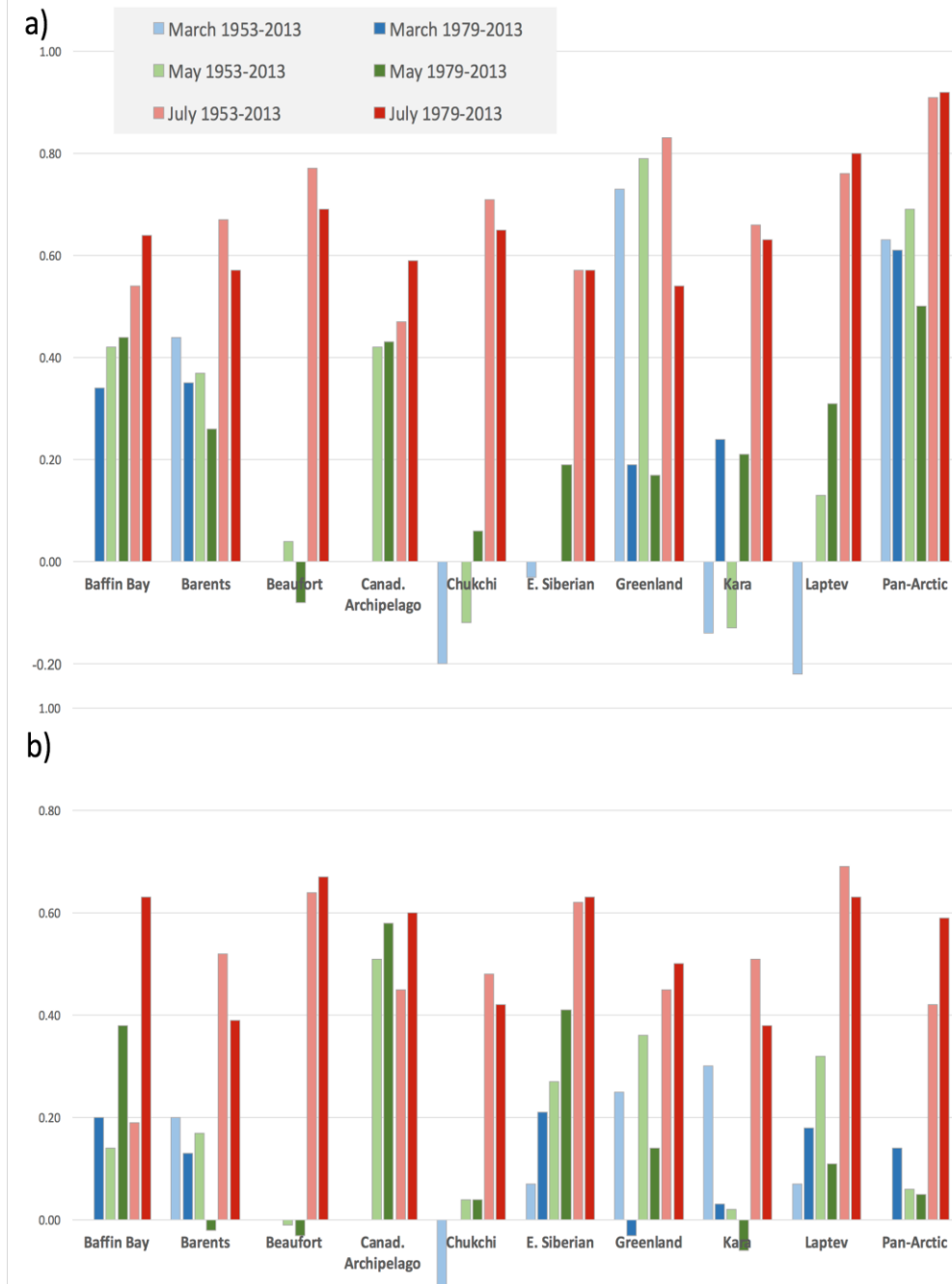
700

701

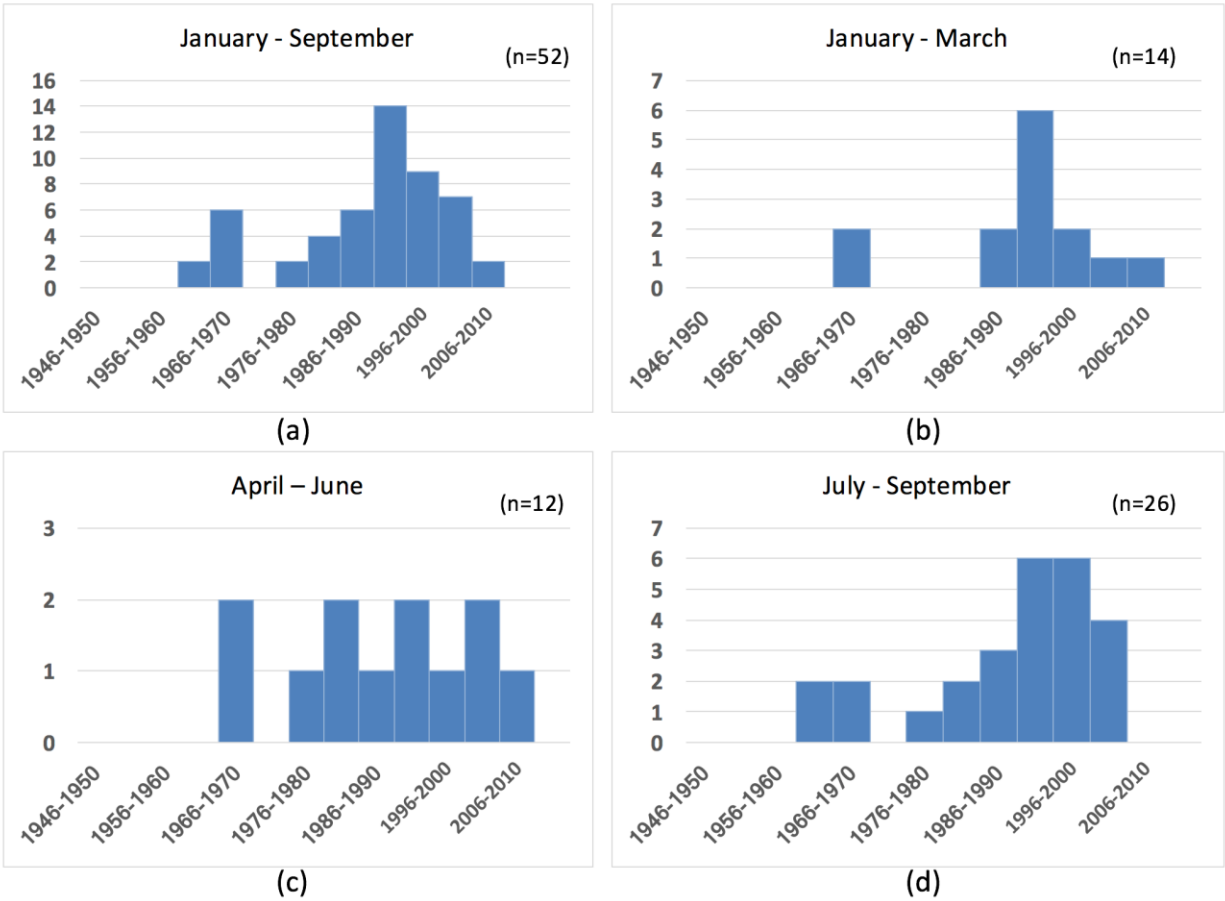


702
 703
 704
 705
 706
 707

Figure 4. Examples of different fit methods (see legend) applied to the BSI (upper panel) and the September Beaufort ice extent time series (lower panel).



708
 709 **Figure 5.** Correlations of September ice extents in individual seas with ice extent in the same
 710 region in March (green bars), May (blue bars) and July (red bars) bases on (a) non-
 711 detrended data and (b) detrended data. Correlations are also shown for Pan-Arctic
 712 extent (far right in each panel). The correlations are based on non-detrended data. For
 713 each color, light-colored bars are for 1953-2013 and dark-colored bars are for 1979-
 714 2013. The absence of a bar indicates a correlation of zero. The 95% significant levels
 715 for the longer and shorter samples are 0.26 and 0.33, respectively.



716

717

718 **Figure 6.** The distribution of break-point years across all regions for (a) January-September and

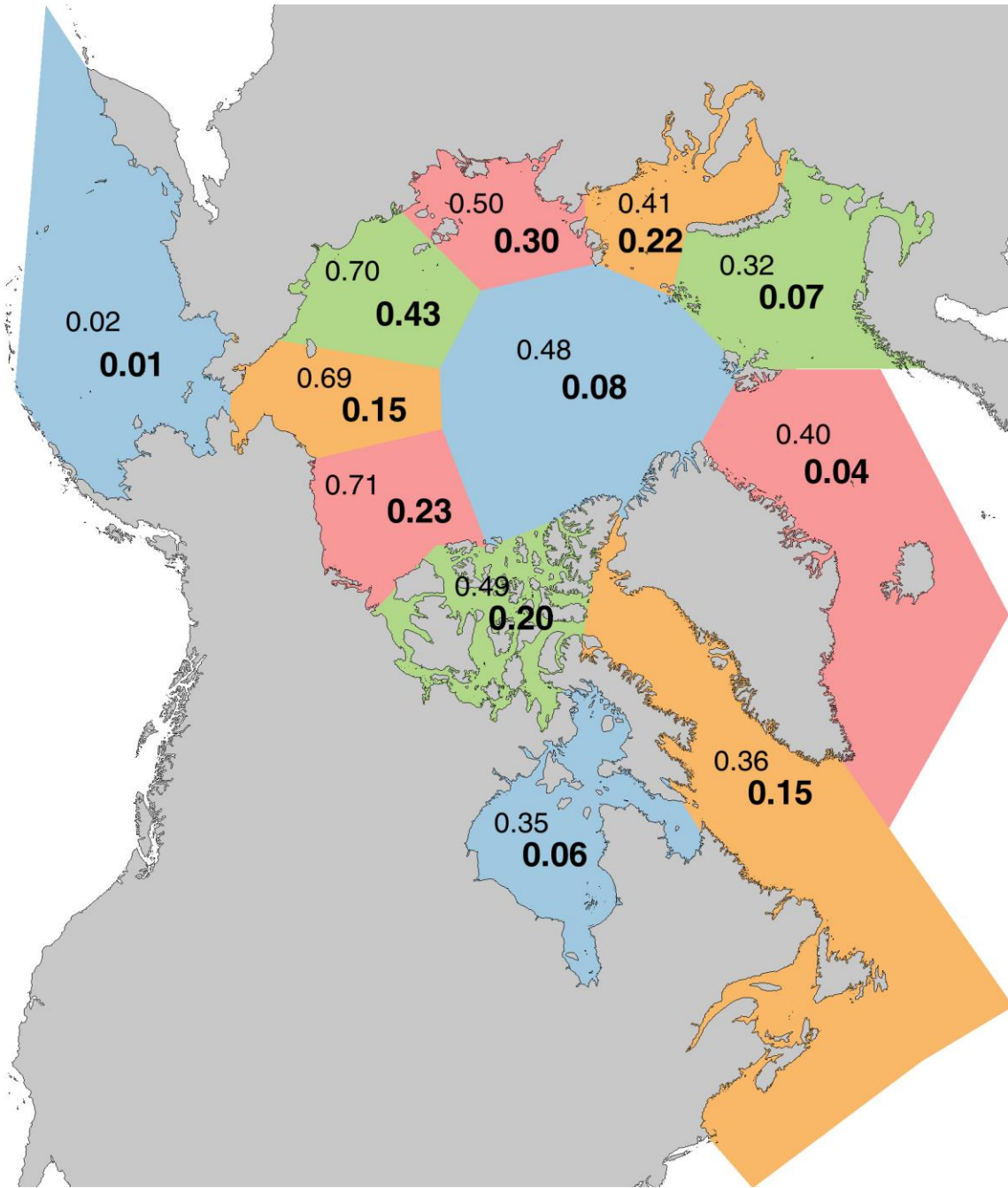
719 its three subperiods: (b) January-March, (c) April-June, (d) July-September). Only

720 cases for which detrending using two lines, rather than one, reduced the root-mean-

721 squares error by 5% or more are included. Note that y-axes have different scales.

722

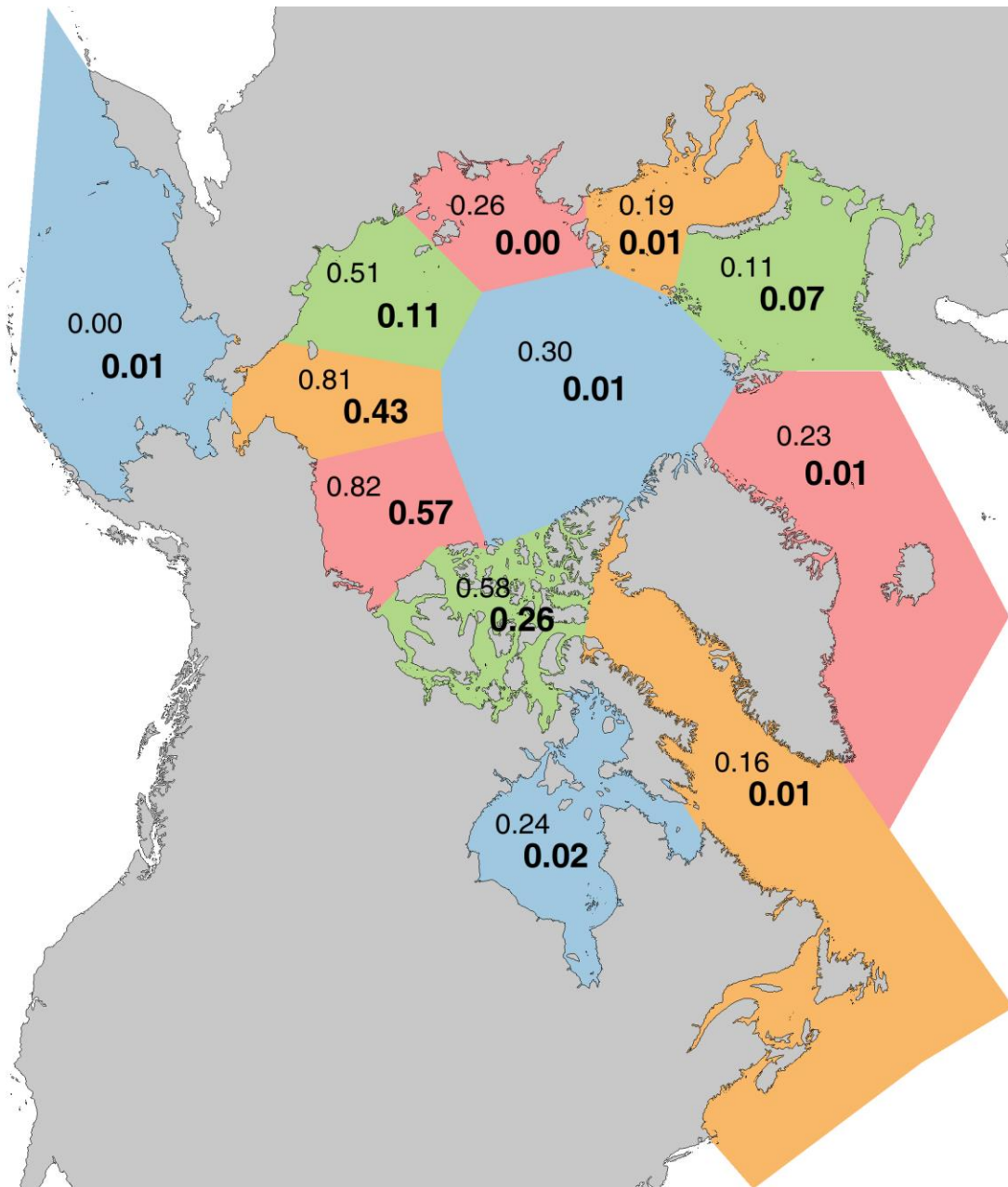
723



724

725

726 **Figure 7.** Squares of correlations (R^2) between September pan-Arctic ice extent and September
 727 regional ice extent based on ice extents including trends (upper numbers in normal
 728 font) and detrended (lower numbers, bold font). The 95% significance thresholds for
 729 the correlations range from 0.26 with no autocorrelation (generally the case for
 730 detrended data) to 0.38 with an autocorrelation of 0.4; the corresponding R^2 thresholds
 731 are 0.07 and 0.14.

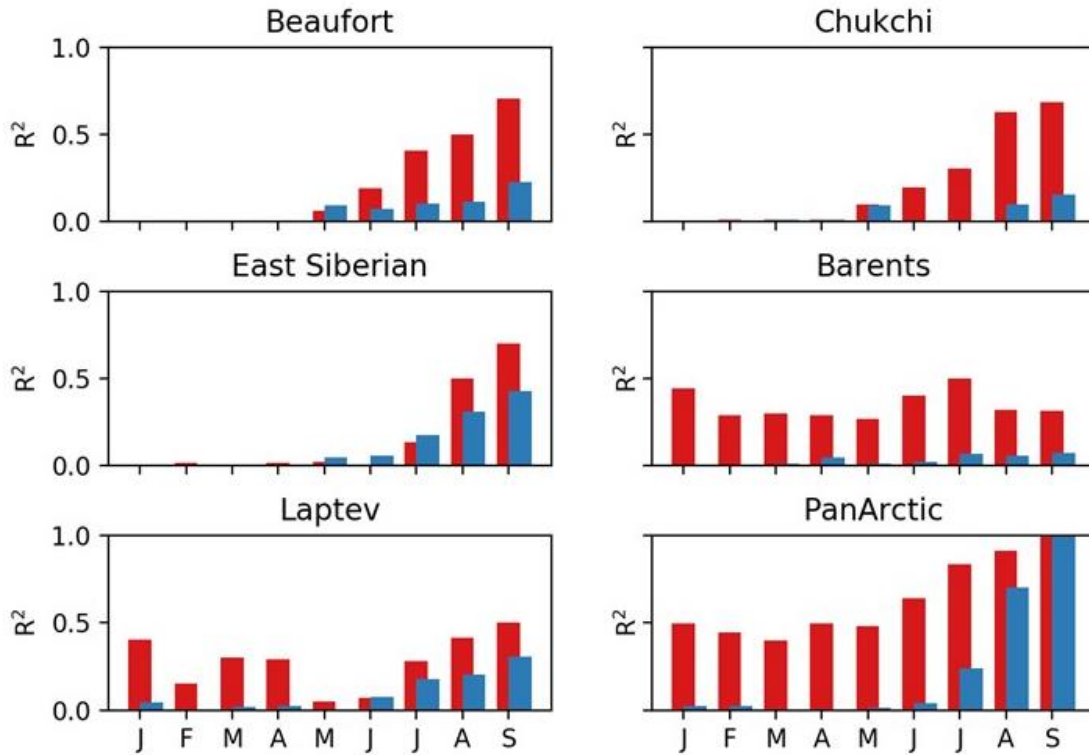


733

734

735 **Figure 8.** As in Figure 7, but for squares of correlations between the annual BSI and September
 736 regional ice extents based on raw (not detrended) time series (upper numbers) and
 737 detrended time series (lower numbers, bold font). The 95% significance thresholds
 738 for the R^2 values range from 0.07 with no autocorrelation (generally the case for
 739 detrended data) to 0.14 with an autocorrelation of 0.4.

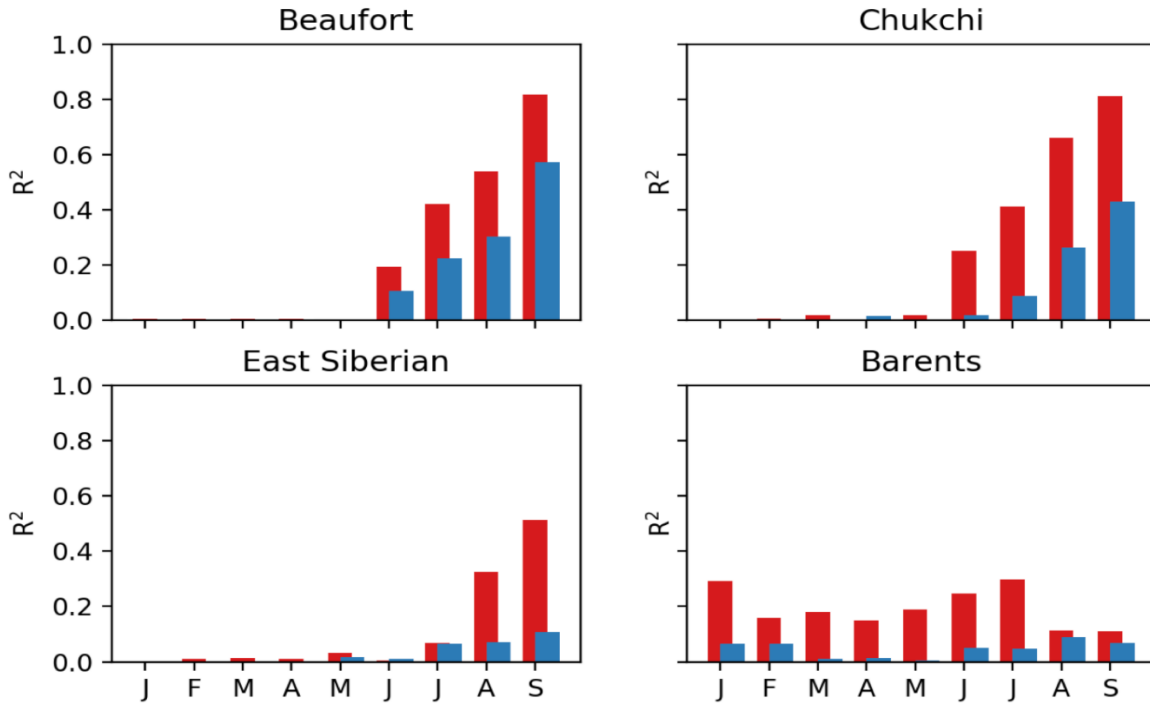
740



742

743 **Figure 9.** Examples of variances of September pan-Arctic ice extent explained by correlations
 744 with antecedent regional ice extent in individual calendar months from September back
 745 to January (pan-Arctic extent lagging by 0, 1, 2, ..., 8 months). Explained variances are
 746 plotted as fractions of explained variance (squares of correlations). Red bars are values
 747 with trends included, blue bars are correlations after removal of trends. The 95%
 748 significance thresholds for the R^2 values range from 0.07 with no autocorrelation
 749 (generally the case for detrended data) to 0.14 with an autocorrelation of 0.4.

750



751

752

753 **Figure 10.** Examples of variances explained by correlations between the Barnett Severity Index
 754 and regional ice extent in individual calendar months from September back to January
 755 (BSI lagging by 0, 1, 2, ..., 8 months). Explained variances are plotted as fractions of
 756 explained variance (squares of correlations). Red bars are values with trends included,
 757 blue bars are correlations after removal of trends. Significance thresholds as in Figure
 758 9.

759

760

Region	Jan	Feb	Mar	Apr	May	Jun	Jul	Aug	Sep
Baffin-St. Lawrence	0.08	0.06	0.02	0.16	0.32	0.49	0.61	0.52	0.36
Barents	0.45	0.29	0.30	0.29	0.27	0.41	0.50	0.32	0.32
Beaufort	0.41	0.41	0.41	0.41	0.06	0.19	0.41	0.50	0.71
Bering	0.00	0.00	0.01	0.00	0.01	0.12	0.08	0.01	0.02
Canadian Archipelago	0.41	0.41	0.41	0.41	0.00	0.13	0.09	0.52	0.49
Central Arctic	0.21	0.11	0.18	0.01	0.02	0.02	0.15	0.07	0.48
Chukchi	0.00	0.01	0.01	0.01	0.10	0.20	0.31	0.63	0.69
East Siberian	0.00	0.02	0.01	0.02	0.02	0.00	0.14	0.50	0.70
Greenland	0.47	0.53	0.50	0.48	0.43	0.41	0.45	0.29	0.40
Hudson	0.05	0.41	0.41	0.26	0.03	0.32	0.66	0.37	0.35
Kara	0.00	0.03	0.11	0.04	0.10	0.09	0.44	0.42	0.41
Laptev	0.40	0.15	0.30	0.29	0.05	0.07	0.28	0.42	0.50
Pan-Arctic	0.50	0.44	0.40	0.50	0.48	0.64	0.84	0.91	1.00

761
762
763
764
765
766
767
768
769
770
771
772

Table 1. Correlations between monthly regional ice extent and pan-Arctic ice extent expressed as explained variance (R^2). Cases where at least 10% of the variance in pan-Arctic ice extent is explained by regional ice extent in a given antecedent month are highlighted with bolded region names. Levels of shading of boxes denote values exceeding 0.10, 0.20, 0.30,...

Region	Jan	Feb	Mar	Apr	May	Jun	Jul	Aug	Sep
Baffin-St. Lawrence	0.09	0.04	0.08	0.06	0.01	0.00	0.03	0.16	0.15
Barents	0.00	0.01	0.01	0.05	0.01	0.02	0.07	0.06	0.07
Beaufort	0.05	0.05	0.05	0.05	0.10	0.08	0.11	0.11	0.23
Bering	0.01	0.01	0.08	0.03	0.02	0.00	0.01	0.01	0.01
Canadian Archipelago	0.05	0.05	0.05	0.05	0.01	0.02	0.02	0.16	0.20
Central Arctic	0.02	0.02	0.11	0.03	0.02	0.04	0.07	0.00	0.08
Chukchi	0.00	0.00	0.01	0.01	0.10	0.00	0.00	0.10	0.15
East Siberian	0.00	0.00	0.00	0.00	0.05	0.06	0.18	0.31	0.43
Greenland	0.06	0.04	0.09	0.07	0.03	0.06	0.04	0.00	0.04
Hudson	0.00	0.05	0.05	0.01	0.05	0.01	0.11	0.07	0.06
Kara	0.01	0.03	0.03	0.04	0.00	0.18	0.12	0.13	0.22
Laptev	0.05	0.00	0.02	0.02	0.01	0.08	0.18	0.21	0.30
Pan-Arctic	0.03	0.02	0.00	0.00	0.01	0.04	0.24	0.70	1.00

773

774

775 **Table 2.** Correlations between detrended monthly regional ice extent and detrended September
776 pan-Arctic ice extent expressed as explained variance (R^2). Cases where at least 10% of the
777 variance in September pan-Arctic ice extent is predictable by regional ice extent in a given
778 antecedent month are highlighted with bolded region names. Shading of boxes is as in Table 1.

1953	7	1984	95
1954	213	1985	24
1955	0	1986	178
1956	0	1987	216
1957	117	1988	0
1958	356	1989	402
1959	163	1990	278
1960	0	1991	3
1961	289	1992	0
1962	195	1993	434
1963	66	1994	1
1964	7	1995	211
1965	10	1996	206
1966	167	1997	407
1967	3	1998	895
1968	412	1999	685
1969	1	2000	513
1970	0	2001	471
1971	34	2002	770
1972	90	2003	827
1973	240	2004	731
1974	22	2005	490
1975	0	2006	819
1976	13	2007	1119
1977	247	2008	12239
1978	46	2009	12989
1979	368	2010	1112
1980	3	2011	1219
1981	74	2012	1298
1982	170	2013	611
1983	0		

Table A1. Yearly values of the Barnett Severity Index (BSI). Source: Rebecca Rolph, Geophysical Institute, University of Alaska, Fairbanks.